Available online at www.sciencedirect.com
ScienceDirect
Polymer 47 (2006) 7085–7094
polymer
www.elsevier.com/locate/polymer

Dynamic mechanical and dielectric relaxation characteristics of poly(trimethylene terephthalate)

Sumod Kalakkunnath, Douglass S. Kalika*

Department of Chemical and Materials Engineering and Center for Manufacturing, University of Kentucky, 177 Anderson Hall (Tower), Lexington, KY 40506-0046, USA

Received 17 July 2006; received in revised form 3 August 2006; accepted 4 August 2006
Available online 30 August 2006

Abstract

The dynamic mechanical and dielectric relaxation properties of a commercial poly(trimethylene terephthalate) [PTT] have been investigated for both quenched and isothermally melt-crystallized specimen films. The relaxation characteristics of PTT were consistent with those of other low-crystallinity semiflexible polymers, e.g. PET and PEEK. While the sub-glass relaxation was largely unperturbed by the presence of the crystalline phase, both calorimetric and broadband dielectric measurements across the glass transition indicated the existence of a sizeable rigid amorphous phase (RAP) fraction in melt-crystallized PTT owing to the constraining influence of the crystal surfaces over the crystal–amorphous interphase region. A strong increase in measured dielectric relaxation intensity ($\Delta\varepsilon$) with temperature above T_g indicated the progressive mobilization of the RAP material, as well as an overall loss of correlation amongst the responding dipoles.

Keywords: Poly(trimethylene terephthalate); Rigid amorphous phase; Dielectric spectroscopy

1. Introduction

Poly(trimethylene terephthalate) [PTT] is a semicrystalline aromatic polyester synthesized by the polycondensation of terephthalic acid and 1,3-propanediol, and is a member of the series of polyesters that includes both poly(ethylene terephthalate) [PET] and poly(butylene terephthalate) [PBT]. PTT did not emerge as a commercial resin until the mid-1990s, owing to advances in the synthesis and economical production of the 1,3-propanediol monomer. Current commercial interest in PTT is focused on fiber and textile products, as well as on other thermoplastic applications.

The appearance of commercial PTT resins has led to renewed interest in the fundamental properties of the polymer and their relation to engineering performance. Numerous studies have appeared that examine the thermal properties of PTT [1–4], its crystal structure [5,6], crystallization kinetics [7–15], and thermal stability [16–20]. In many respects, the thermal and relaxation characteristics of PTT are intermediate to the properties of PET and PBT, and are typical of those encountered with semiflexible polymers of low to medium crystallinity [21–29]. According to Pyda et al. [1], PTT can be quenched under liquid nitrogen to a low-crystallinity state (weight fraction crystallinity ~ 14%), with a corresponding calorimetric glass transition temperature (T_g) of about 42 °C. In thermally crystallized PTT, the constraining influence of the crystals leads to a positive offset in T_g by as much as 15 °C as compared to the quenched polymer, depending on the details of the sample. Heat capacity measurements indicate the presence of a distinct rigid amorphous phase (RAP) fraction in PTT that relaxes with increasing temperature [2]: the amount of rigid amorphous phase is a function of prior crystallization history, with fractions as large as 0.33 observed for cold-crystallized specimens. The reported equilibrium melting temperature for PTT is approximately 237 °C, with a corresponding 100% crystalline heat of fusion equal to 30 kJ mol^{-1} [1].

* Corresponding author. Tel.: +1 859 257 5507; fax: +1 859 323 1929.
E-mail address: kalika@engr.uky.edu (D.S. Kalika).

0032-3861/$ - see front matter © 2006 Elsevier Ltd. All rights reserved.
doi:10.1016/j.polymer.2006.08.005

In this paper, we report the dynamic mechanical and dielectric relaxation characteristics of quenched and melt-crystallized PTT. Data are presented for samples prepared by direct quenching in liquid N_2, as well as for a series of isothermally melt-crystallized films with controlled thermal history. Of particular interest is the influence of crystallinity on the glass–rubber relaxation characteristics of PTT, and the emergence of rigid amorphous phase fraction in this material.

2. Experimental

PTT polymer was obtained in pellet form through the courtesy of Shell Chemical Company, Houston, TX (CORTERRA™ PTT 200). The as-received pellets were dried at 90 °C under vacuum for 24 h, and then stored over desiccant at room temperature until further use. Sample films (0.25–0.50 mm thickness) were prepared by compression molding the pellets in a Carver melt press: the polymer was held in the melt at 260 °C for approximately 5 min during the molding. Quenched specimens were obtained by transferring the incipient films directly from the melt press to an enclosed bath of liquid nitrogen, and the resulting samples were stored under refrigeration at 4 °C to minimize potential aging effects. Isothermally crystallized films were prepared by transferring the polymer from the melt press to a second, adjacent press held at the desired crystallization temperature. Isothermal annealing temperatures for melt crystallization ranged from 160 °C to 200 °C. An annealing time of 1 h was ample for full crystallization of the samples, as confirmed by calorimetry. At the conclusion of the one-hour annealing time, the samples were removed from the melt press and allowed to cool under ambient conditions (25 °C). The melt-crystallized films were subsequently held under vacuum at room temperature prior to measurement.

Calorimetric studies were performed on both the quenched and isothermally crystallized films using a Perkin–Elmer DSC-7 differential scanning calorimeter. Transition temperatures and melting enthalpy were calibrated using indium and zinc standards. A sapphire (Al_2O_3) reference was used for the calibration of heat capacity in the vicinity of the glass transition temperature [30]; determination of heat capacity was accomplished according to the method detailed by Wunderlich [31]. All DSC scans were performed at a heating rate of 10 °C min^{-1}, with a sample size of 10 mg.

Wide-angle X-ray scattering (WAXS) was employed for the investigation of the crystal structure in the quenched and selected melt-crystallized films. Samples were examined using a Siemens 5000 diffractometer with Cu K_α radiation ($\lambda = 1.5406$ Å) at room temperature. Data were recorded across a range of scattering angles (2θ) from 5 to 50°; the scan rate was 2° min^{-1}, with a data interval of 0.02°.

Dynamic mechanical analysis (DMA) was performed using a Polymer Laboratories dynamic mechanical thermal analyzer operating in single cantilever bending geometry; the polymer films had a thickness of 0.50 mm. Storage modulus (E') and loss tangent ($\tan\delta$) were recorded at a heating rate of 1 °C min^{-1} with test frequencies in the range of 0.1–10 Hz; all measurements were carried out under inert (N_2) atmosphere.

Dielectric spectroscopy measurements were conducted using the Novocontrol Concept 40 broadband dielectric spectrometer (Hundsangen, Germany). Concentric silver electrodes were vacuum evaporated on the crystallized samples using a VEECO thermal evaporation system. For the quenched PTT films, electrodes were deposited at room temperature using silver paint (SPI Supplies, West Chester, PA). Samples were mounted between gold platens and positioned in the Novocontrol Quatro Cryosystem; sample thickness was 0.25 mm in all cases. Dielectric constant (ε') and loss (ε'') were recorded in the frequency domain from 0.1 Hz to 1.0 MHz at discrete temperatures from −150 °C to 150 °C.

3. Results and discussion

3.1. Calorimetric studies

DSC heating sweeps for the quenched and isothermally melt-crystallized PTT sample films are reported in Fig. 1. The quenched film shows a glass transition centered at 44 °C, followed by a sharp cold crystallization exotherm (67 °C) and melting at 227 °C. In the isothermally melt-crystallized samples, the glass transition is shifted to ~54 °C, with T_g displaying virtually no dependence on prior crystallization temperature. An expanded view of the DSC curves in the vicinity of the glass transition is shown in Fig. 2.

The DSC heating sweeps for the melt-crystallized PTT samples show a characteristic double-melting behavior, with a lower-temperature melting peak positioned approximately 10 °C above the isothermal annealing temperature, followed by an apparent crystal re-organization process and second melting peak at ~227 °C. Multiple melting behavior has been reported for a wide range of flexible and semiflexible crystalline polymers and is typically attributed to the existence of distinct crystal lamellar populations, or the onset of crystal melting and ongoing re-crystallization during the DSC heating scan itself. In a detailed analysis presented by Srimoaon et al.

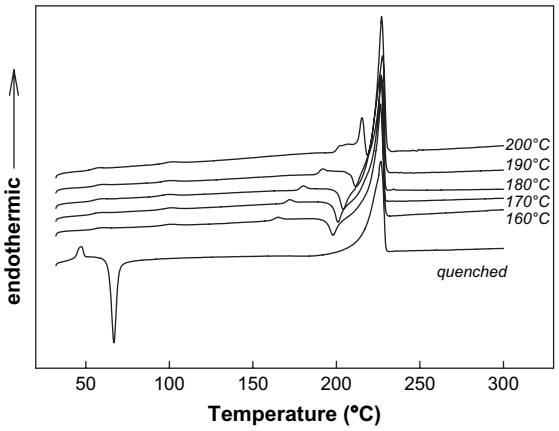

Fig. 1. DSC heating sweeps (10 °C min^{-1}) for quenched and isothermally melt-crystallized PTT.

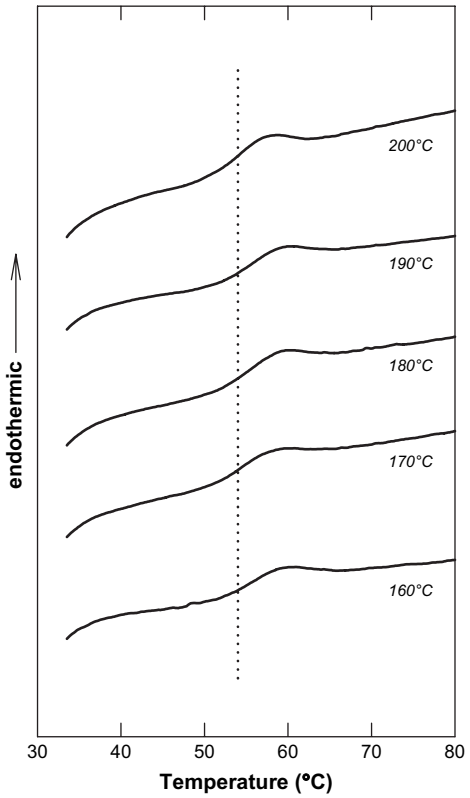

Fig. 2. DSC heating sweeps (10 °C min^{-1}) for isothermally melt-crystallized PTT: expanded view of glass transition region.

[4], multiple melting phenomena in PTT were attributed primarily to simultaneous melting and re-crystallization over the course of the DSC scan. This conclusion is consistent with the form of the curves shown in Fig. 1, wherein the position of the higher-temperature melting peak ($T_m = 227$ °C) is independent of prior isothermal crystallization temperature and reflects the conditions of re-organization during the DSC heating sweep.

In addition to the "double-melting" peaks described above, a small endothermic melting feature is evident in the DSC scans at 100 °C for all of the semicrystalline specimens. This peak, with a corresponding enthalpy of ~0.2 kJ mol^{-1}, appears to reflect a small amount of additional crystallization that occurs in the samples when they are removed from the melt press and allowed to cool to room temperature after isothermal annealing.

The enthalpy associated with each calorimetric event was determined in order to establish the net heat of fusion (ΔH_F) and corresponding weight fraction crystallinity present in the individual PTT samples. For the liquid nitrogen quenched film, comparison of the crystallization and melting peaks in the DSC sweep indicates the presence of 13 wt% residual crystallinity in the original sample, which is very close to the value reported by Pyda et al. [1]. This appears to be the minimum level of crystallinity captured in this commercial PTT resin, even under aggressive quenching conditions. Complementary studies involving the melting and direct liquid nitrogen quenching of PTT samples held in sealed aluminum DSC pans showed similar levels of residual crystallinity. For the isothermally melt-crystallized films, the weight fraction crystallinity across the various samples was $W_C = 0.30 \pm 0.02$, with no systematic variation in crystallinity evident as a function of prior crystallization temperature.

The crystallinity characteristics of the PTT films were also examined by wide-angle X-ray scattering (WAXS) measurements. Fig. 3 shows diffraction patterns for the quenched film and for a representative melt-crystallized film prepared at $T_c = 180$ °C. The diffraction pattern for the quenched film is essentially featureless, suggesting that the minimal crystallinity ($W_C = 0.13$) present in the quenched specimen cannot be differentiated from the amorphous halo. Thus, WAXS does not provide any additional information regarding the amount or character of the residual crystallinity present in the quenched film. The melt-crystallized specimen, however, shows a distinct diffraction pattern that closely matches WAXS results reported in the literature [5,6]: the Miller indices included in Fig. 3 correspond to a triclinic unit cell, with dimensions as reported in Ref. [6].

The presence of crystallinity in semiflexible polymers typically leads to a positive offset in T_g owing to the constraining influence of the crystals on the large-scale segmental motions inherent to the glass–rubber transition. This behavior has been observed in a number of polymers for which wholly amorphous specimens can be obtained by rapid quenching to the glassy state; e.g., PET [22,32], poly(phenylene sulfide) [PPS] [24,28], and poly(ether ether ketone) [PEEK] [23,25,26]. The measured offset in the glass transition temperature is usually in the range of 10–15 °C. A similar result is observed for the quenched and melt-crystallized PTT samples examined here ($\Delta T = +10$ °C), even though the quenched PTT resin could not be captured in the 100% amorphous state. In addition to its influence on T_g, the presence of crystallinity

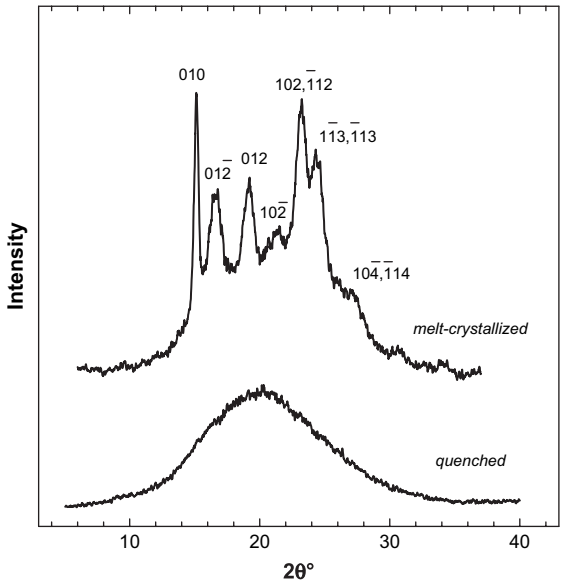

Fig. 3. Wide-angle X-ray diffraction patterns (intensity versus 2θ) for quenched and melt-crystallized ($T_c = 180$ °C) PTT; Cu K_α radiation, $\lambda = 1.5406$ Å. Indexing of diffraction peaks as per Ref. [6].

often results in a disproportionate decrease in the intensity of the glass transition, as measured by the step change in heat capacity, $\Delta C_p(T_g)$. The disproportionate decrease in ΔC_p for crystalline samples as compared to a wholly amorphous specimen can be quantified using a three-phase morphological model that includes a separate *rigid amorphous* phase fraction, i.e., a portion of the non-crystalline material that remains "rigid" at the glass transition and thus does not contribute to the observed increase in heat capacity observed at T_g. If the mobile amorphous phase fraction (W_{MA}) is defined as:

$$W_{MA} = \frac{\Delta C_p^{SC}(T_g)}{\Delta C_p^{A}(T_g)} \quad (1)$$

where ΔC_p^{SC} corresponds to the measured heat capacity increment for the semicrystalline sample, and ΔC_p^{A} corresponds to the heat capacity increment for the wholly amorphous material, it then follows that the rigid amorphous phase fraction can be determined by the difference

$$W_{RAP} = 1 - W_{MA} - W_C \quad (2)$$

with the weight fraction crystallinity (W_C) established from X-ray or calorimetric measurements.

In Fig. 4, $\Delta C_p(T_g)$ for the various crystallized PTT samples is plotted versus the value of the net heat of fusion (ΔH_F) following the approach presented in Ref. [1]. The dashed line reflects the limit for a strictly two-phase model, where the intensity of the glass transition is directly proportional to the amount of non-crystalline phase present in the sample; the limiting values for ΔC_p and ΔH_F are the result of extrapolations reported by Pyda and co-workers [1]. Data points that fall below the dashed line correspond to samples wherein the intensity of the glass transition is less than what would be anticipated according to a strictly two-phase response, and thus can be interpreted using a three-phase model that includes a separate rigid amorphous phase fraction. For the thermally crystallized samples investigated here, the data are clustered well below the two-phase limit, suggesting the existence of a sizeable amount of RAP material, with W_{RAP} in the range of 0.3–0.4. There does not appear to be any clear correlation between RAP fraction and crystallization temperature for this particular group of samples. The corresponding RAP values are comparable to W_{RAP} fractions for PTT reported by Hong et al. [33], where phase fraction determinations were based on both DSC and small-angle X-ray studies.

3.2. Dynamic mechanical analysis

Dynamic mechanical heating scans were performed on quenched PTT films and isothermally melt-crystallized specimens. Results for a quenched film are shown in Fig. 5. The sample displays two distinct mechanical relaxation processes: a sub-glass process (designated as the β relaxation), centered at −70 °C (1 Hz; see inset in Fig. 5), followed by the glass transition (α relaxation), with an onset temperature of approximately 50 °C. The glass–rubber relaxation results in a dramatic decrease in the storage modulus (E') of the quenched sample. However, the onset of cold crystallization during the DMA heating sweep leads to a sharp recovery in the modulus, followed by additional (broader) relaxation of the semicrystalline specimen above 80 °C (refer to Fig. 5).

The origin of sub-glass relaxations in poly(*n*-methylene terephthalates) has been the subject of considerable interest. Early dynamic mechanical measurements across a series of such polyesters with $n = 2$ (PET) up to $n = 10$ indicated a complex character for the observed β relaxation, which appeared to encompass at least two superimposed loss processes [34]. More recent studies on the secondary relaxation behavior of PTT have similarly indicated overlapping mechanical relaxations across the sub-glass range [35,36]. Maxwell and co-workers performed ^{13}C and deuterium NMR studies [37], as well as dynamic mechanical and dielectric measurements [38], in order to elucidate the underlying sub-glass molecular motions in amorphous PET. A comparison of their dielectric and dynamic mechanical data indicated that the dielectric (β) peak was the result of a single relaxation process, while

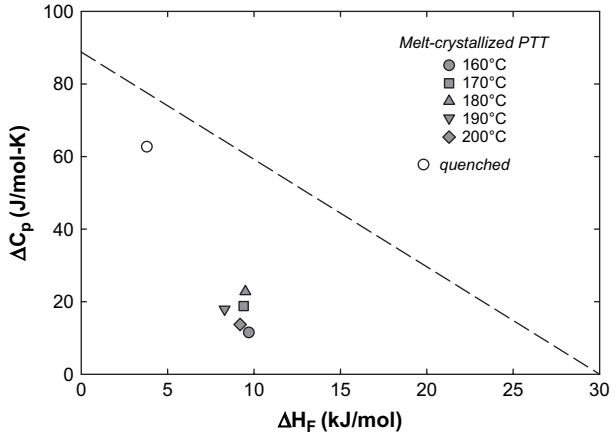

Fig. 4. Incremental increase in heat capacity ($\Delta C_p(T_g)$; J/mol K) versus net heat of fusion (ΔH_F; kJ/mol) for melt-crystallized PTT.

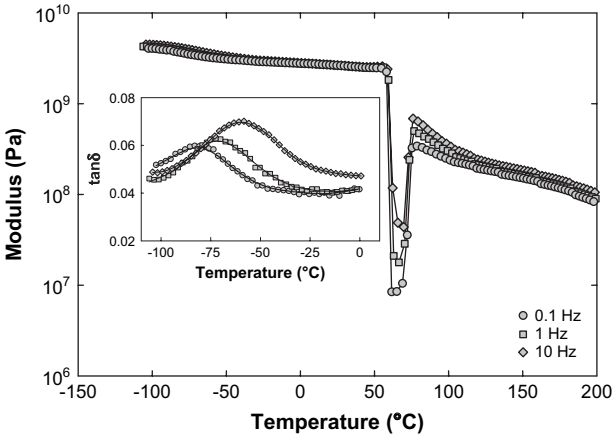

Fig. 5. Dynamic mechanical storage modulus (E'; Pa) versus temperature for quenched PTT; heating rate of 1 °C min^{-1}. Inset: tan δ versus temperature for sub-glass (β) transition region.

the dynamic mechanical peak encompassed two apparent motional processes. The dielectric relaxation, which corresponds to the low-temperature side of the dynamic mechanical peak, was assigned to localized motion of the carbonyl groups. The high-temperature side of the dynamic mechanical peak was the result of (dielectrically inactive) phenyl ring motions, as corroborated by NMR. Similar behavior is observed for our PTT specimens: a direct comparison of the dynamic mechanical and dielectric results for quenched PTT is provided in Section 3.3.

Dynamic mechanical data for a representative melt-crystallized PTT specimen ($T_c = 160\ ^\circ C$) are presented in Fig. 6. In the crystallized PTT sample, the glass–rubber (α) relaxation is much broader than that observed in the quenched film, and reflects the heterogeneous character of the relaxation environment in the semicrystalline material. Time–temperature superposition [39] was used to construct a modulus–frequency master curve for crystalline PTT in the vicinity of the glass transition: a reference temperature of 80 °C was selected, which corresponds to the position of the dynamic mechanical tan δ peak at a frequency of 1 Hz. The result for the $T_c = 160\ ^\circ C$ sample is shown in Fig. 7, where the data are plotted as storage modulus versus ωa_T, where ω is the applied test frequency ($\omega = 2\pi f$, with f expressed in Hz) and a_T is the dimensionless shift factor. The inset to Fig. 7 shows the shift factor plotted as a function of temperature: the a_T data display a temperature dependence consistent with the WLF (Williams–Landel–Ferry) relation [39].

The glass–rubber relaxation in crystalline PTT could be satisfactorily described using the Kohlrausch–Williams–Watts (KWW) "stretched exponential" relaxation time distribution function:

$$\phi(t) = \exp\left[-(t/\tau_o)^{\beta}\right] \quad (3)$$

where τ_o is the observed relaxation time and β is the distribution parameter. β ranges from 0 to 1, with values close to unity corresponding to a narrow, single relaxation time (Debye) response. Lower values of β reflect increased inter-molecular coupling, as well as inhomogeneous relaxation broadening owing to the presence of physical or chemical crosslinks. Series approximations reported by Williams et al. express modulus and loss for the KWW model in the frequency domain [40]: the best-fit relaxation curve based on these equations is shown in Fig. 7. A distribution parameter value (β) of 0.14 was obtained for isothermally melt-crystallized PTT prepared at 160 °C.

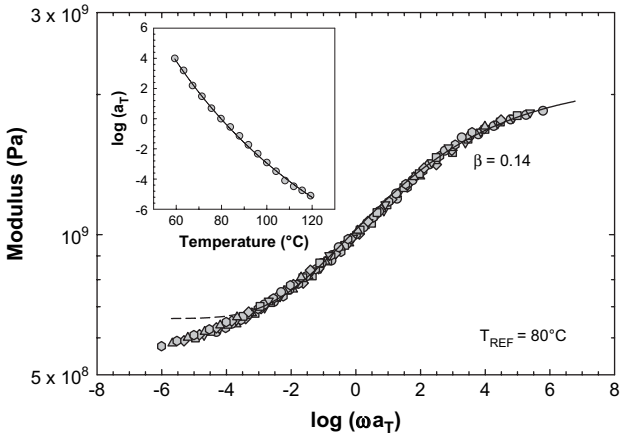

Fig. 7. Time–temperature master curve for melt-crystallized ($T_c = 160\ ^\circ C$) PTT; $T_{REF} = 80\ ^\circ C$. Solid curve is KWW best fit. Inset: time–temperature shift factor (a_T) versus temperature.

Dynamic mechanical results for the various melt-crystallized PTT samples are compared across the glass transition region in Fig. 8. As discussed above, the thermal histories imposed in this study (i.e., isothermal melt crystallization at temperatures ranging from 160 °C to 200 °C) produced only minimal differences in the bulk crystallinity of the resulting materials. Similarly, the dynamic mechanical tan δ curves for these specimens show very little variation as a function of crystallization condition, with relaxation peak temperature and intensity nearly invariant for the different films. For samples crystallized at lower temperatures (160 °C and 170 °C), the relaxation appears to be somewhat broader, especially on

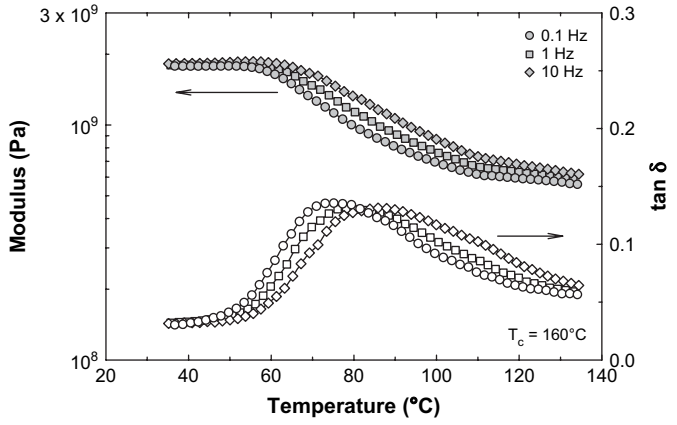

Fig. 6. Dynamic mechanical storage modulus (filled symbols) and tan δ (empty symbols) versus temperature for melt-crystallized ($T_c = 160\ ^\circ C$) PTT; heating rate of 1 °C min^{-1}.

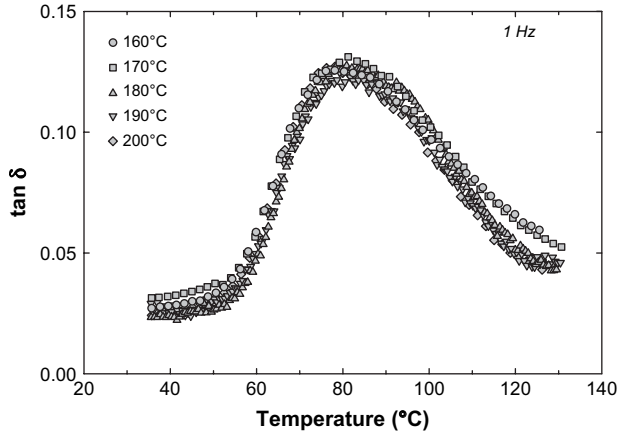

Fig. 8. Dynamic mechanical tan δ versus temperature for melt-crystallized PTT. Frequency of 1 Hz; heating rate of 1 °C min^{-1}.

the high-temperature side of the relaxation peak. This suggests a broader distribution of relaxation environments in these samples, and may reflect poorer crystal organization owing to the deep quench intervals experienced by the films during preparation.

3.3. Dielectric spectroscopy

Dielectric results for quenched PTT are plotted in Fig. 9 as dielectric constant (ε') and loss (ε'') versus temperature at selected frequencies from 0.1 Hz to 1 MHz. The data show a broad low-temperature relaxation (β relaxation), and then a sharp increase in permittivity that corresponds to large-scale dipolar mobilization at the glass transition (α relaxation). The glass transition is followed by an abrupt, frequency-independent decrease in dielectric constant that reflects the onset of cold crystallization in the quenched specimen and the corresponding immobilization and/or constraint of some fraction of the responding dipoles with increased bulk crystallinity. The presence of cold crystallinity leads to a positive offset in the nominal glass transition temperature of the test specimen, as well as a broadening of the glass–rubber relaxation. The completion of the offset glass transition process at higher temperatures (>70 °C) is evident as a gradual increase in ε', and as a broad high-temperature shoulder in ε''. Similar features in dielectric constant and loss have been reported for quenched PET [22], PPS [41,42] and PEEK [25,27,43].

Dielectric results for isothermally melt-crystallized PTT ($T_c = 170$ °C) are reported in Fig. 10. In this case, two distinct incremental increases in dielectric constant are evident, corresponding to the sub-glass (β) and glass–rubber (α) relaxations; the features of the glass transition are not complicated by the effects of additional crystallization during measurement. The dielectric loss peak at the glass transition is considerably broadened as compared to the quenched sample, as the polymer chains experience a much wider spectrum of segmental relaxation environments. The observed increases in dielectric constant and loss at lower test frequencies and higher temperatures correspond to the onset of Maxwell–Wagner–Sillars (MWS) interfacial polarization owing to the accumulation of mobile charge carriers at the interfaces between the crystal and amorphous phases [44].

The dielectric dispersions for both the glass–rubber and sub-glass relaxations were analyzed according to the Havriliak–Negami (HN) modification of the single relaxation time Debye expression [45,46]:

$$\varepsilon^* = \varepsilon_U + \frac{\varepsilon_R - \varepsilon_U}{\left[1 + (i\omega\tau_{HN})^a\right]^b} \tag{4}$$

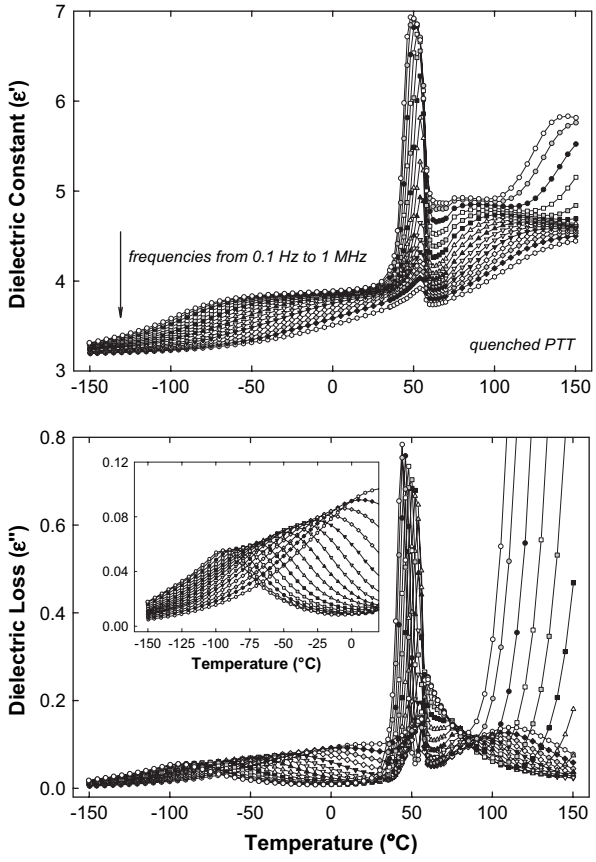

Fig. 9. Dielectric constant (ε') and loss (ε'') versus temperature for quenched PTT; selected frequencies from 0.1 Hz to 1 MHz. Inset: expanded view of dielectric loss across the sub-glass transition region.

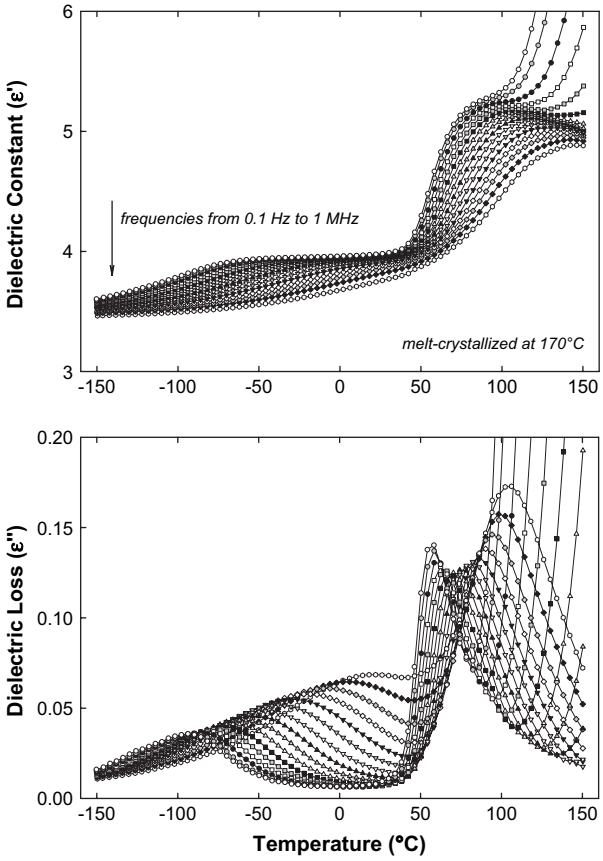

Fig. 10. Dielectric constant (ε') and loss (ε'') versus temperature for melt-crystallized ($T_c = 170$ °C) PTT; selected frequencies from 0.1 Hz to 1 MHz.

where ε_R and ε_U represent the relaxed ($\omega \to 0$) and unrelaxed ($\omega \to \infty$) values of the dielectric constant, $\omega = 2\pi f$ is the frequency, τ_{HN} is the central relaxation time, and a and b represent the broadening and skewing parameters, respectively. All (HN) curve fits reported here were performed using the WinFit software program provided with the Novocontrol dielectric instrument.

Dielectric loss data are plotted as a function of frequency for quenched PTT in Fig. 11. Across the glass transition region, there is a narrow temperature range (44–56 °C) for which satisfactory HN curve fits can be obtained without the influence of cold crystallization. Results for a representative melt-crystallized sample ($T_c = 170$ °C) are provided in Fig. 12. In each case (α and β relaxations), the loss data in the frequency domain were fit with a single HN function. The HN curve fits were used to establish the frequency associated with the maximum in dielectric loss (f_{MAX}), and the dielectric relaxation intensity ($\Delta\varepsilon = \varepsilon_R - \varepsilon_U$) as a function of temperature.

The time–temperature characteristics for the α and β relaxations are presented as an Arrhenius plot of log(f_{MAX}) versus 1000/T(K) in Fig. 13, with data corresponding to the quenched sample and selected melt-crystallized films. For the β relaxation, the localized motions, which are presumably associated with reorientation of carbonyl groups, follow a linear

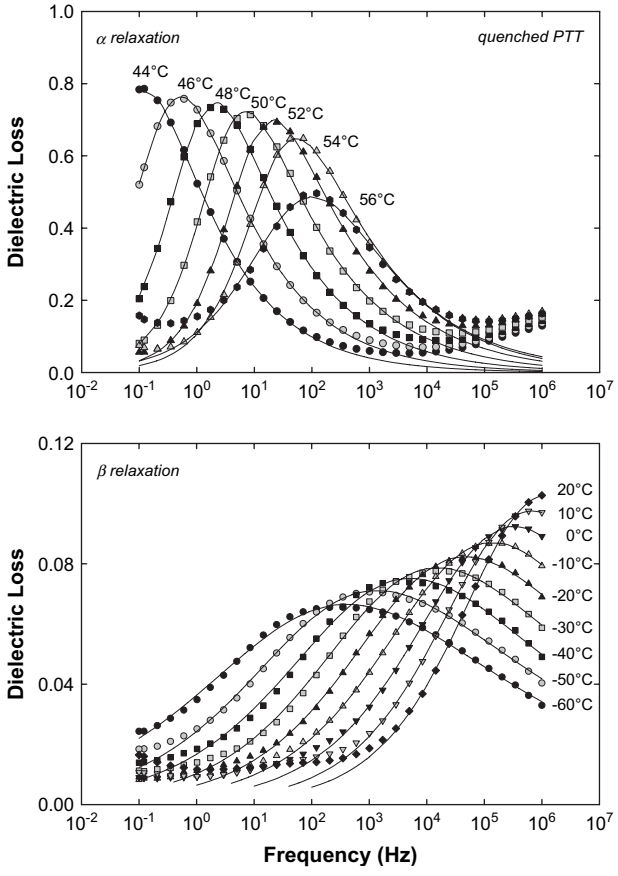

Fig. 11. Dielectric loss (ε'') versus frequency for quenched PTT across the glass–rubber (α) and sub-glass (β) relaxation regions. Solid curves are Havriliak–Negami best fits.

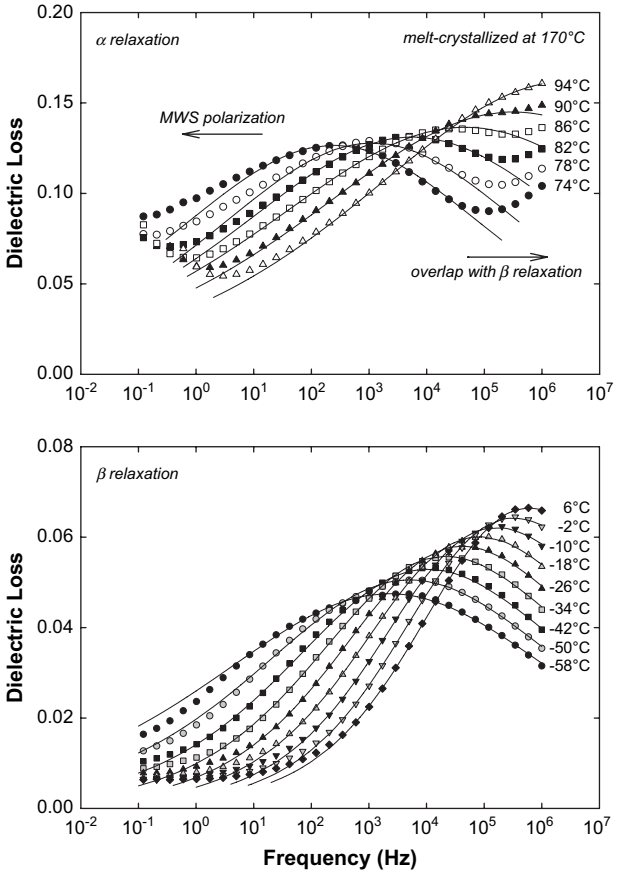

Fig. 12. Dielectric loss (ε'') versus frequency for melt-crystallized ($T_c = 170$ °C) PTT across the glass–rubber (α) and sub-glass (β) relaxation regions. Solid curves are Havriliak–Negami best fits.

Arrhenius relation which is typical of sub-glass relaxations in polymers [47]. The position of the β relaxation is nearly independent of the sample morphology (i.e., quenched versus melt-crystallized samples), reflecting the localized character of the dipolar reorientations. The apparent activation energy (E_A) determined from the slope of the dielectric Arrhenius plot is 54 kJ mol^{-1} for the quenched sample, which is close to values reported for both PET [48,49] and PBT [50]. The

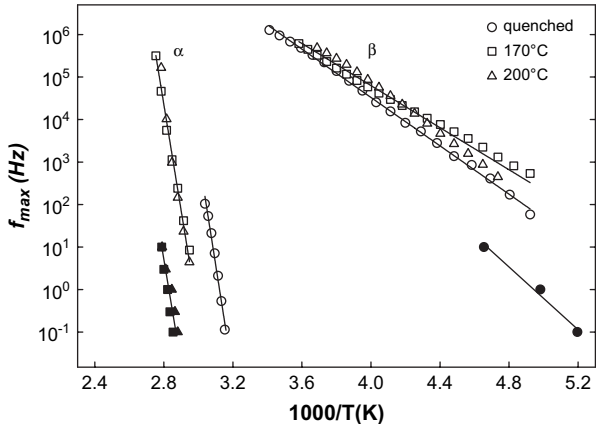

Fig. 13. Arrhenius plot of f_{MAX} (Hz) versus 1000/T(K) for quenched and melt-crystallized PTT. (○) Quenched; (□) $T_c = 170$ °C; (△) $T_c = 200$ °C. Empty symbols: dielectric results. Filled symbols: dynamic mechanical results.

results for the dielectric α relaxation in Fig. 13 clearly reflect the positive offset in glass transition temperature that is observed with the presence of melt crystallinity in the PTT samples. Over the range of frequencies investigated, the data for both the quenched and crystallized films can be described by a single activation energy; $E_A = 485$ kJ mol^{-1}.

Examination of the dielectric and DMA data for quenched PTT shows that the sub-glass dynamic mechanical loss peak is offset to higher temperatures relative to the dielectric β relaxation (refer to Fig. 13). A direct comparison of the tan δ curves for quenched PTT at a frequency of 1 Hz is provided in Fig. 14. As discussed above, previous dielectric and dynamic mechanical studies on PET have suggested that the sub-glass dielectric relaxation corresponds to a single (lower temperature) process that reflects motion of the carbonyl groups, while the dynamic mechanical peak encompasses two processes; i.e., carbonyl motions, as well as (higher temperature) phenyl ring flips [38]. The PTT tan δ curves shown in Fig. 14 are consistent with this scenario, with the dielectric probe sensitive to only a subset of the local motions that comprise the overall sub-glass relaxation response.

The HN curve fits reported in Figs. 11 and 12 were used to establish the dielectric relaxation intensities for the β and α relaxations as a function of temperature and thermal history. Fig. 15 reports Δε versus temperature for quenched and melt-crystallized PTT. Comparison of Δε for the β relaxation indicates an overall decrease in relaxation intensity by 25% for the melt-crystallized samples relative to the quenched film, which is consistent with the measured increase in bulk crystallinity, W_C, from 0.13 to 0.30. Previous studies on PET samples encompassing a wide range of crystallinity indicated that the intensity of the sub-glass relaxation varies directly with the fraction amorphous phase present in the samples, which implies that the localized sub-glass motions that occur in the amorphous regions are unperturbed by the presence of the crystallites [22,51]. The PTT results presented here indicate a similar behavior, although the range of crystallinities encompassed by the PTT samples is not sufficient to establish a definitive relationship between dielectric relaxation intensity and fraction crystallinity.

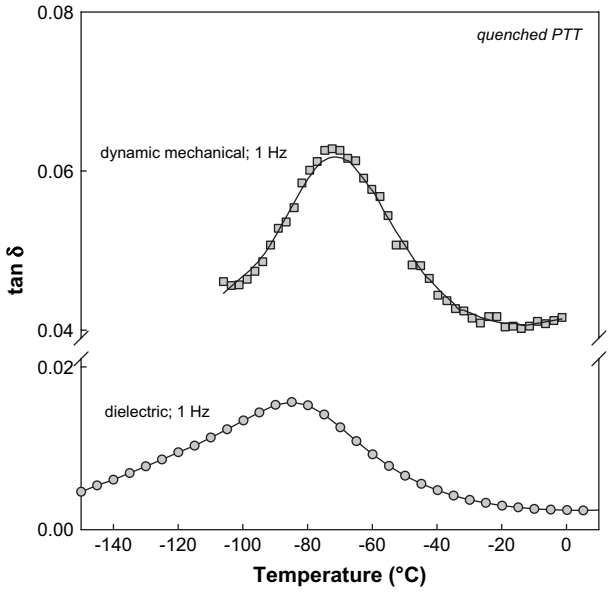

Fig. 14. Comparison of tan δ versus temperature curves for quenched PTT; frequency of 1 Hz.

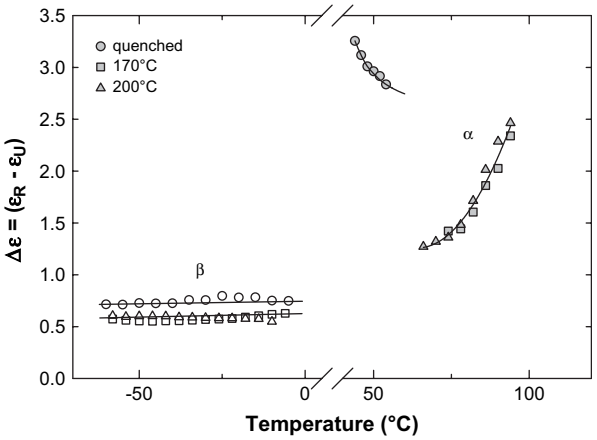

Fig. 15. Dielectric relaxation intensity ($\Delta\varepsilon = \varepsilon_R - \varepsilon_U$) versus temperature for quenched and melt-crystallized PTT; sub-glass (β) and glass–rubber (α) relaxations.

The PTT dielectric relaxation intensity across the α relaxation is a strong function of temperature for both the quenched and melt-crystallized materials; see Fig. 15. In quenched PTT, dielectric relaxation intensity for the glass transition can be determined across a relatively narrow range of measurement temperatures prior to the onset of cold crystallization. Over this range, Δε decreases steadily with temperature in a manner that has been reported for a number of similar polymers; e.g. PET [22], PPS [41,42] and PEEK [25,43]. For the melt-crystallized PTT samples, the dielectric relaxation intensity is reduced substantially below the value that might be expected based on a strictly two-phase morphological model wherein only those chain segments incorporated into the crystalline phase are held immobile in the range between T_g and crystal melting. This again suggests the presence of a sizeable rigid amorphous phase fraction in these samples, with the constraining influence of the crystals extending well into the amorphous phase. The comparison of dielectric relaxation intensity for the semicrystalline samples ($\Delta\varepsilon^{SC}$) relative to the value for a wholly amorphous specimen ($\Delta\varepsilon^{A}$) provides an alternate route for the determination of mobile amorphous phase fraction, W_{MA}. However, the calculation is complicated by a number of factors, including the availability of an experimental value for a 100% amorphous PTT sample, as well as the strong temperature dependence of Δε observed for both the quenched and crystallized materials; this issue is addressed in detail for PEEK in Ref. [25]. Using a quenched sample value for Δε equal to 2.7 (and adjusting for residual crystallinity), the mobile amorphous phase fraction for isothermally crystallized PTT is calculated to be $W_{MA} \sim 0.45$ at 70 °C. This corresponds to a rigid amorphous phase fraction, $W_{RAP} = 0.25$.

At temperatures above T_g, the dielectric relaxation intensity measured for the melt-crystallized samples increases strongly with temperature. This behavior, which has been observed to

varying extents in the other polymers cited above, may reflect a gradual mobilization of the rigid amorphous phase with increasing temperature, as well as a reduction in local dipolar correlation of the ester groups. The extent of dipolar correlation is typically expressed via the Onsager–Kirkwood correlation factor, g [47,52], which accounts for the influence of intra- and inter-molecular correlations on the response of the individual constituent dipoles and can reflect local dipolar cancellations as well as spatial restrictions to dipolar orientation [53]. In PTT, the increase in $\Delta\varepsilon$ with temperature above T_g appears to be exceptionally strong, and may reflect not only the progressive mobilization of ''rigid amorphous'' segments in the crystal–amorphous interphase, but also the disruption of local dipolar cancellations owing to an increase in overall conformational mobility, thus leading to a larger net dipolar response.

4. Conclusions

The thermal and dynamic relaxation characteristics of quenched and melt-crystallized poly(trimethylene terephthalate) have been investigated. Quenching PTT from the melt state into liquid N_2 resulted in films with a residual crystalline fraction, $W_C = 0.13$; fully amorphous samples could not be obtained for the PTT resin examined in this study. Isothermal melt crystallization at temperatures ranging from 160 to 200 °C led to a bulk crystallinity of ~0.30, independent of crystallization temperature. The presence of melt crystallinity produced a positive offset in the glass transition temperature ($\Delta T = 10$ °C), and calorimetry measurements revealed the existence of a sizeable rigid amorphous phase fraction in the melt-crystallized samples. Dynamic mechanical analysis and broadband dielectric spectroscopy were used to study the sub-glass and glass–rubber relaxation characteristics of quenched and crystalline PTT. The relaxation properties of PTT were consistent with the behavior reported for other semi-flexible polymers such as PET, PPS and PEEK. The sub-glass (β) relaxation in PTT was largely unperturbed by the presence of crystallinity. Comparison of the dynamic mechanical and dielectric sub-glass relaxations suggested that the dielectric response reflected a lower-temperature subset of the motions that were encompassed in the broader, more complex mechanical relaxation. For the glass–rubber (α) relaxation, dielectric measurements showed a strong influence of crystallinity on the resulting dielectric relaxation intensity, again consistent with the presence of a significant amount of rigid amorphous material in the melt-crystallized specimens. The strong increase in measured relaxation intensity with temperature above T_g suggested a gradual mobilization of the rigid amorphous phase, as well as an overall loss of dipolar correlation.

Acknowledgements

This work was supported in part through a Major Research Equipment Grant awarded by the Office of the Vice President for Research at the University of Kentucky, and a Kentucky Opportunity Fellowship administered by the University of Kentucky Graduate School. Assistance with sample preparation and calorimetry measurements was provided by Mr. Terry Humphries with support from the University of Kentucky Office of Undergraduate Studies. We are pleased to acknowledge Shell Chemical Company (Westhollow Technology Center) for providing the polymer resin used in this work.

References

[1] Pyda M, Boller A, Grebowicz J, Chuah H, Lebedev BV, Wunderlich B. J Polym Sci Part B Polym Phys 1998;36:2499–511.
[2] Pyda M, Wunderlich B. J Polym Sci Part B Polym Phys 2000;38:622–31.
[3] Chung W-T, Yeh W-J, Hong P-D. J Appl Polym Sci 2002;83:2426–33.
[4] Srimoaon P, Dangseeyun N, Supaphol P. Eur Polym J 2004;40:599–608.
[5] Ho R-M, Ke K-Z, Chen M. Macromolecules 2000;33:7529–37.
[6] Wang B, Li CY, Hanzlicek J, Cheng SZD, Geil PH, Grebowicz J, et al. Polymer 2001;42:7171–80.
[7] Huang J-M, Chang F-C. J Polym Sci Part B Polym Phys 2000;38:934–41.
[8] Chuah HH. Polym Eng Sci 2001;41:308–13.
[9] Hong P-D, Chung W-T, Hsu C-F. Polymer 2002;43:3335–43.
[10] Supaphol P, Dangseeyun N, Srimoaon P, Nithitanakul M. Thermochim Acta 2003;406:207–20.
[11] Dangseeyun N, Srimoaon P, Supaphol P, Nithitanakul M. Thermochim Acta 2004;409:63–77.
[12] Supaphol P, Apiwanthanakorn N. J Polym Sci Part B Polym Phys 2004;42:4151–63.
[13] Xue M-L, Sheng J, Yu Y-L, Chuah HH. Eur Polym J 2004;40:811–8.
[14] Zhang J. J Appl Polym Sci 2004;93:590–601.
[15] Sahay SS, Krishnan K. Thermochim Acta 2005;430:23–9.
[16] Wang X-S, Li X-G, Yan D. Polym Degrad Stab 2000;69:361–72.
[17] Wang X-S, Li X-G, Yan D. Polym Test 2001;20:491–502.
[18] Wang X-S, Li X-G, Yan D. J Appl Polym Sci 2002;84:1600–8.
[19] Ramiro J, Eguiazabal JI, Nazabal J. J Appl Polym Sci 2002;86:2775–80.
[20] Kelsey DR, Kiibler KS, Tutunjian PN. Polymer 2005;46:8937–46.
[21] Boyd RH. Polymer 1985;26:323–47.
[22] Coburn JC, Boyd RH. Macromolecules 1986;19:2238–45.
[23] Cheng SZD, Cao M-Y, Wunderlich B. Macromolecules 1986;19:1868–76.
[24] Cheng SZD, Wu ZQ, Wunderlich B. Macromolecules 1987;20:2802–10.
[25] Kalika DS, Krishnaswamy RK. Macromolecules 1993;26:4252–61.
[26] Krishnaswamy RK, Kalika DS. Polymer 1994;35:1157–65.
[27] Krishnaswamy RK, Kalika DS. Polymer 1996;37:1915–23.
[28] Wu SS, Kalika DS, Lamonte RR, Makhija S. J Macromol Sci Phys 1996;B35:157–78.
[29] Kalika DS. Dielectric spectroscopy of crystalline polymers and blends. In: Nalwa HS, editor. Handbook of low and high dielectric constant materials and their applications. San Diego: Academic Press; 1999. p. 275–327.
[30] Furukawa GT, Douglas TB, McCoskey RE, Ginnings DC. J Res Natl Bur Stand 1956;57:67–82.
[31] Wunderlich B. Thermal analysis. San Diego: Academic Press; 1990.
[32] Ilers KH, Breuer H. J Colloid Sci 1963;18:1–31.
[33] Hong P-D, Chuang W-T, Yeh W-J, Lin T-L. Polymer 2002;43:6879–86.
[34] Farrow G, Macintosh J, Ward IM. Makromol Chem 1960;38:147–58.
[35] Gonzalez CC, Perena JM, Bello A. J Polym Sci Part B Polym Phys 1988;26:1397–408.
[36] Mackintosh AR, Liggat JJ. J Appl Polym Sci 2004;92:2791–6.
[37] Maxwell AS, Ward IM, Laupretre F, Monnerie L. Polymer 1998;39:6835–49.
[38] Maxwell AS, Monnerie L, Ward IM. Polymer 1998;39:6851–9.
[39] Ferry JD. Viscoelastic properties of polymers. 3rd ed. New York: John Wiley and Sons; 1980.
[40] Williams G, Watts DC, Dev SB, North AM. Trans Faraday Soc 1971;67:1323–35.

[41] Huo P, Cebe P. J Polym Sci Part B Polym Phys 1992;30:239–50.
[42] Kalika DS, Wu SS, Lamonte RR, Makhija S. J Macromol Sci Phys 1996; B35:179–97.
[43] Huo P, Cebe P. Macromolecules 1992;25:902–9.
[44] Schonhals A, Kremer F. Analysis of dielectric spectra. In: Kremer F, Schonhals A, editors. Broadband dielectric spectroscopy. New York: Springer-Verlag; 2003. p. 59–98.
[45] Havriliak S, Negami S. J Polym Sci Polym Symp 1966;14:99–103.
[46] Havriliak S, Havriliak SJ. Dielectric and mechanical relaxation in materials. Cincinnati: Hanser; 1997.
[47] McCrum NG, Read BE, Williams G. Anelastic and dielectric effects in polymeric solids. London: John Wiley and Sons; 1967.
[48] Tatsumi T, Eiko I, Hayakawa R. J Polym Sci Part B Polym Phys 1992;30: 701–6.
[49] Pop T, Iordache D, Jonas A. Microelectron Eng 1997;33:377–84.
[50] Pratt GJ, Smith MJA. J Mater Sci 1990;25:477–81.
[51] Dobbertin J, Hensel A, Schick C. J Therm Anal 1996;47:1027–40.
[52] Schonhals A, Kremer F. Theory of dielectric relaxation. In: Kremer F, Schonhals A, editors. Broadband dielectric spectroscopy. New York: Springer-Verlag; 2003. p. 1–33.
[53] Boyd RH, Liu F. Dielectric spectroscopy of semicrystalline polymers. In: Runt JP, Fitzgerald JJ, editors. Dielectric spectroscopy of polymeric materials. Washington, DC: American Chemical Society; 1997. p. 107–36.